Electronic transport in doped $SrTiO_3$: Conduction mechanisms and potential applications

A. Spinelli, M. A. Torija, C. Liu, C. Jan, and C. Leighton*
Department of Chemical Engineering and Materials Science, University of Minnesota, Minneapolis, Minnesota 55455, USA
(Received 29 January 2010; revised manuscript received 24 March 2010; published 14 April 2010)

Resistivity, Hall effect, and magnetoresistance are reported on a large set of semiconducting $SrTiO_{3-\delta}$ single crystals doped *n*-type (by reduction or Nb substitution) over a broad range of carrier density (the 10^{15} to mid 10^{20} cm^{-3} range). Temperature-independent carrier densities, strongly temperature-dependent mobilities (up to 22 000 $cm^2\ V^{-1}\ s^{-1}$ at 4.2 K), and a remarkably low critical carrier density for the metal-insulator transition are observed, and interpreted in terms of the known quantum paraelectricity of the host. We argue that an unusual, high mobility, low density, metallic state is thus established at carrier densities at least as low as 8.5×10^{15} cm^{-3}, in contrast to some prior conclusions. At low temperatures, the temperature dependence of the mobility and resistivity exhibit a nonmonotonic carrier density dependence and an abrupt change in character near 2×10^{16} cm^{-3}, indicating a distinct crossover in conduction mechanism, perhaps associated with a transition from impurity-band to conduction-band transport. The results provide a simple framework for the understanding of the global transport behavior of doped $SrTiO_3$. Finally, it is proposed that the large residual resistivity ratios (>3000), and large, temperature independent, Hall coefficients (>1700 $cm^3\ C^{-1}$), demonstrate considerable potential for high-sensitivity resistive thermometry and Hall sensing applications.

DOI: 10.1103/PhysRevB.81.155110 PACS number(s): 72.20.−i, 71.30.+h

I. INTRODUCTION

The perovskite oxides have been the focus of over 50 years of investigation, primarily due to their wide-ranging functionality and the fascinating interplay between their crystal structures and properties. $SrTiO_3$ (STO) is a classic example. This compound crystallizes in the cubic $Pm\bar{3}m$ space group at room temperature (with a lattice parameter of 3.905 Å), undergoing a symmetry-lowering transition to a tetragonal structure below 105 K.[1] Historically, both in terms of applications and basic research, the primary interest in this material derives from its unusual dielectric properties. The dielectric constant (ε_r) is strongly temperature and electric field dependent, increasing from around 300 at 300 K to tens of thousands at low temperatures.[2–5] The exact origins of this complex temperature dependence and the nature of the ground state have been the subject of several decades of intensive study. In general terms, STO is believed to be a quantum paraelectric, with quantum fluctuations suppressing the onset of spontaneous electric polarization despite proximity to a ferroelectric instability, resulting in flattening of $\varepsilon_r(T)$ at low temperature and large deviations from Curie-Weiss behavior.[2–5]

The majority of the research discussed above focused on bulk crystals of STO. Recent years have witnessed an increasing interest in the use of this material in thin films and heterostructures. This is driven partially by potential application as a dielectric layer in data storage devices[6–9] or as a component in superconductor-based microwave devices,[10] and partially by the growing basic interest in complex oxide heterostructures.[11,12] In addition to its widespread use as a single-crystal substrate for epitaxial growth of oxides (due to its commercial availability, controllable surface termination,[13–16] and close lattice match to numerous complex oxide materials[11–18]), STO has also been employed as an active component in oxide heterostructures and thin films. Examples include its use as an insulating barrier layer in manganite-based magnetic tunnel junctions,[19–21] as a dielectric layer in field-effect devices for tuning the carrier density of materials such as manganites and cuprates,[22–26] and in such systems as $SrTiO_3/LaAlO_3$ superlattices where interface metallicity has been observed[27–30] and ascribed to formation of a two-dimensional electron gas.[27] Control of epitaxial strain in thin films has even been used to artificially stabilize a ferroelectric ground state.[31]

Of most relevance to this work, STO also displays fascinating, and potentially useful, electronic transport properties. The material is a semiconductor with a 3.2 eV band gap[1,32] and can be doped *n* type [32–44] or *p* type.[45–51] *n*-type conduction has been most commonly achieved by substitution of La^{3+} for Sr^{2+} (i.e., $Sr_{1-x}La_xTiO_3$),[1,33,34] Nb^{5+} for Ti^{4+} (i.e., $SrTi_{1-y}Nb_yO_3$),[35–37] or by reduction to $SrTiO_{3-\delta}$,[32,35,38–44] where, in a simple picture, each O vacancy generates two doped electrons. Similarly, *p*-type doping has been achieved by substituting trivalent metal ions (e.g., In^{3+}, Al^{3+}, Fe^{3+}, and Sc^{3+}) for Ti^{4+}.[45–51] Electronic-transport measurements were reported as early as 1964,[38] with detailed studies of reduced and Nb-substituted samples appearing from 1967,[32,35,41,42] although they reported significant discrepancies between groups. Even at this early stage, enough was known about the dielectric response to relate certain features of the transport to the large, temperature-dependent, ε_r. For example, in certain doping ranges, multiple studies observed an almost temperature-independent Hall coefficient,[32,35,38,41] which was rationalized in terms of the large ε_r. Within the hydrogenic theory of shallow donors (the appropriateness of such a model for STO will be discussed below), the donor binding energy, E_D, and Bohr radius, a_B, are given by

$$E_D = -13.6\ \text{eV}\left(\frac{m_e^*}{m_e}\right)\left(\frac{1}{\varepsilon_r^2}\right), \quad a_B = 0.53\ \text{Å}(\varepsilon_r)\left(\frac{m_e}{m_e^*}\right), \tag{1}$$

where m_e^* and m_e are the effective and free-electron masses, respectively. Even with the unusually high (and potentially

temperature-dependent[38]) m_e^* of $1m_e-10m_e$, Eq. (1) predicts E_D of order 1.5 meV at 300 K decreasing to 0.2 μeV at 4.2 K. This simple picture places doped STO in an unfamiliar regime where shallow donors remain ionized at essentially all temperatures of interest, explaining the absence of "carrier freeze-out." At lower carrier densities however, freeze-out *was* observed in several studies,[32,35,38,42] behavior that remains poorly understood. The low-temperature mobility (μ) in early studies was scattered over a very wide range (from 4 to 30 000 $cm^2\ V^{-1}\ s^{-1}$) (Refs. 32, 35, 38, 41, and 42) but was nevertheless unexpectedly high. This was again interpreted in terms of the large $\varepsilon_r(T)$, which is naively expected to generate highly effective screening of ionized impurity scattering centers. Both of the most commonly employed models (i.e., the Conwell-Weiskopf[52] and Brooks-Herring[53] models) predict that the ionized impurity mobility, μ_{II}, varies approximately as ε_r^2, resulting, in the case of very high ε_r, in a total mobility, $\mu=(1/\mu_{II}+1/\mu_{phonon})^{-1}$, that is phonon limited. Nevertheless, attempts to quantitatively understand $\mu(T)$ in doped STO were not entirely successful,[32,35,41,42] although the important role of soft transverse-optical phonon modes was established.[54] It should be noted at this point that although the simple hydrogenic picture is qualitatively compatible with many of the experimental results, the appropriateness of such an approach has been questioned. Epifanov and Levanyuk[56] pointed out that the nonlinearity of the dielectric response is important and can lead to a situation where the strong temperature dependence of the static ε_r has little impact on the impurity ionization energy. This point will be returned to below.

Interest in the electronic transport in STO was further stimulated by the discovery of a dome of superconductivity in the temperature-carrier density (n) plane, with transition temperatures up to 0.3–0.4 K,[57,58] as well as certain ingredients known to induce unconventional superconductivity.[59] As pointed out by Ohtomo and Hwang,[60] it is quite remarkable that the transition from insulator to superconductor in $SrTiO_{3-\delta}$ can be induced by only 0.03% of O vacancies. This transition from insulator to superconductor has now been electrostatically tuned[61] while experiments on ultrathin Nb-doped films have demonstrated both two-dimensional (2D) superconductivity and Shubnikov-de Haas oscillations.[62] In addition, it has been pointed out that the quantum paraelectricity enables access to the extreme quantum limit of magnetotransport at sufficiently low n.[63] Given this significant interest in electronic transport in doped STO, and the considerable gaps in our understanding of the fundamental conduction processes and structure-property relationships, it is clearly worthwhile to make additional detailed studies in high-quality bulk single crystals. In particular, issues such as the presence (or otherwise) of carrier freeze-out, the unexplained carrier density dependence of the mobility, scattering mechanisms, and even issues as fundamental as the position of the metal-insulator transition (MIT) (Ref. 64) are far from clear at this point.

In the present paper, we revisit the electronic-transport properties of reduced and Nb-substituted n-type STO. The availability of high-quality commercial single crystals (both undoped and Nb substituted) significantly simplifies the work, enabling investigation of a large set of crystals, over a wide doping range, while minimizing uncontrolled sample-to-sample variations. A comprehensive set of resistivity (ρ), Hall coefficient (R_H), mobility (μ), and magnetoresistance (MR) data have been acquired (from 0.4 to 350 K) over a much wider range of carrier densities (10^{15} to $>10^{20}$ cm^{-3}) than previous reports, enabling us to assemble a complete understanding of the electronic-transport properties. We observe a high-mobility metallic state with strongly temperature-dependent resistivity, which persists down to the lowest carrier densities probed, in the absence of carrier freeze-out. The very low critical carrier density for the MIT (which is found to be very different than that concluded from some prior work), and the unusual metallic state, are discussed as consequences of the large $\varepsilon_r(T)$ resulting from the quantum paraelectric behavior. With increasing n, we observe unusual nonmonotonic behavior of the low-temperature transport and a clear change in the character of the conduction process near 2×10^{16} cm^{-3}, which can be interpreted in terms of a crossover from impurity-band (IB) to conduction-band (CB) transport. Based on these unconventional electronic properties, we also suggest some possible applications of doped $SrTiO_3$. In particular, we propose that this material has significant application potential in high-sensitivity resistive thermometry [for resistance temperature detectors (RTDs) or calorimeters], and for high-sensitivity Hall sensing.

II. EXPERIMENTAL DETAILS

Single-crystal samples, grown by the Verneuil method and post annealed at 1700 C for 48 h, were purchased from two vendors [Crystal GmbH (Ref. 65) and MTI (Ref. 66)] and verified single crystal by x-ray diffraction. These substrates have (001) orientation and were polished to the typical specifications for epitaxial growth but were not treated further.[13–16] The samples were screened based on the full width at half maximum (FWHM) of the rocking curves through the [002] peak, a parameter that exhibits considerable sample-to-sample variations in commercial STO substrates. Data presented in this paper were taken on samples with a single rocking curve peak with typical FWHM of $0.03°-0.06°$. Nb-doped samples with doping concentrations of $N_{Nb}=0.02$, 0.2, 1.00, 1.40, and 2.00 at. % were investigated. Lower carrier densities were obtained by reduction, which, for most of the samples, was performed in a UHV system equipped with a residual gas analyzer. Oxygen partial pressures were kept to $P_{O_2}\leq1\times10^{-9}$ Torr, the extent of reduction being controlled by the reduction temperature (T_{Red}). The reduction time was in the range 0.5–2.0 h. A small number of samples were reduced at much higher temperature (1100 °C) in a conventional tube furnace in a vacuum of order 10^{-6} Torr. Both Nb-doped and reduced samples were investigated by room-temperature high-resolution wide-angle x-ray diffraction, which found no evidence of secondary phase formation. As an example, 2 at. % Nb-doped samples exhibited a barely detectable increase in lattice parameter over pristine STO of around 0.001 Å, consistent with the larger Nb^{5+} ionic radius. Remarkably, the reduced samples also showed a similar increase in lattice parameter

TABLE I. Doping and transport parameters for 19 doped $SrTiO_3$ samples. The parameters are the 300 K carrier density [n(300 K)], the Nb dopant concentration (N_{Nb}), the ratio of carrier density to Nb concentration (n/N_{Nb}), the reduction temperature (T_{Red}), the 300 K resistivity [ρ(300 K)], the 4.2 K resistivity [ρ(4 K)], the residual resistivity ratio [RRR=ρ(300 K)/ρ(4 K)], and the 4.2 K mobility [μ(4 K)]. As shown in Fig. 3(b), the lowest temperatures for mobility measurements sometimes exceeded 4.2 K. In this case, we show the value at the lowest temperature measured.

n (300 K) (cm^{-3})	N_{Nb} (at. %)	n/N_{Nb}	T_{Red} (°C)	ρ(300 K) (Ω cm)	ρ (4 K) (Ω cm)	RRR	μ (4 K) ($cm^2\ V^{-1}\ s^{-1}$)
3.8×10^{15}	N/A	N/A	650	2.24×10^{3}	4.31×10^{4}	0.05	
8.53×10^{15}	N/A	N/A	700	1.13×10^{3}	2.18×10^{3}	0.51	
3.76×10^{15}	N/A	N/A	700	9.15×10^{2}			
	N/A	N/A	700	5.41×10^{2}	81.6	6.61	
1.04×10^{16}	N/A	N/A	620	2.22×10^{2}	22.1	9.23	17.1
	N/A	N/A	650	98.3	4.07	24.1	
1.98×10^{16}	N/A	N/A	650	89.1	7.87×10^{-1}	113.2	
2.93×10^{16}	N/A	N/A	670	39.3	1.11×10^{-2}	2140	
5.64×10^{16}	N/A	N/A	600	18.2	8.40×10^{-3}	2580	17700
1.69×10^{17}	N/A	N/A	690	5.08	2.13×10^{-3}	2390	8800
2.13×10^{17}	N/A	N/A	700	3.87	1.63×10^{-3}	2370	18100
	N/A	N/A	1100	2.71	1.00×10^{-3}	2710	
7.76×10^{17}	0.02	0.23	N/A	1.23	2.88×10^{-4}	3010	22100
2.23×10^{18}	N/A	N/A	1100	4.47×10^{-1}	3.14×10^{-4}	1430	3790
	N/A	N/A	1100	1.15×10^{-1}	2.39×10^{-4}	481	
2.72×10^{19}	0.20	0.81	N/A	3.43×10^{-2}	6.73×10^{-5}	493	2370
1.80×10^{20}	1.40	1.07	N/A	5.70×10^{-3}	5.20×10^{-5}	371	570
1.56×10^{20}	1.00	0.66	N/A	6.90×10^{-3}	9.50×10^{-5}	122	469
3.79×10^{20}	2.00	1.11	N/A	2.41×10^{-3}	3.65×10^{-5}	84.8	316

of 0.001–0.002 Å. An increased Ti-O bond length due to improved screening of the repulsive interactions by free carriers or a small amount of reduction to Ti^{3+} are possible sources of this increase.

Transport measurements were performed on $5\times5\times0.5$ mm samples in the van der Pauw geometry. Resistance anisotropy for the samples shown in this work was less than 1.5–2 at all T. All but the most resistive samples were measured using 13.7 Hz ac excitation; more resistive samples were measured dc. Indium was found to make an acceptable Ohmic contact only in the high-n regime. Lower doped samples used sputter-deposited NiCr contacts, which were Ohmic to the lowest temperatures measured at sufficiently small excitation current. Hall measurements were made in the range −2 to 2 T while the MR (with the field perpendicular to the plane) was measured to 9 T. The Hall voltage displayed no discernible deviations from linearity with field in the entire temperature, field, and doping range investigated, and the sign of the Hall coefficient was consistent with electrons as the charge carriers.

III. RESULTS AND DISCUSSION

A detailed summary of the doping parameters and transport properties of 19 samples (both reduced and Nb-substituted) is provided in Table I. The Nb-doped samples cover the range from $n=8\times10^{17}$ to 4×10^{20} cm^{-3}, corresponding to 300 K resistivity values from 1 to 10^{-3} Ω cm. A comparison between the measured electron densities and those expected assuming one doped electron per Nb donor atom (n/N_{Nb} in Table I) reveals that the samples with $N_{Nb}\geq0.2$ at. % all have $n\approx N_{Nb}$, consistent with all Nb dopants being electrically active, ionized (see discussion below), and with an insignificant density of compensating acceptors. (Note that simple estimates demonstrate that the intrinsic carrier density of STO is negligible for this discussion). The 0.02 at. % Nb sample however has $n/N_{Nb}=0.23$, i.e., considerably less than 1. This could be due to some electrically inactive Nb dopants, or the presence of compensating acceptors of unknown origin, as in prior work.[32,35,38,41,42] Assuming complete ionization we estimate that an acceptor density of 10^{17}–10^{18} cm^{-3} would be sufficient to explain the behavior of these Nb-doped samples. $SrTiO_{3-\delta}$ samples were obtained using T_{Red} values from 600 to 1100 °C, resulting in carrier densities from the low 10^{15} to mid 10^{18} cm^{-3} region. The presence or otherwise of compensating acceptors in the reduced samples is not known from any of the measurements presented in this work, although in the low-n samples it is very likely that significant compensation occurs.[32,35,38,41,42] The reduced samples have 300 K resistivities from $>10^{3}$ to 10^{-1} Ω cm. As discussed in more detail below, there is thus a significant range of overlap between the reduced and Nb-

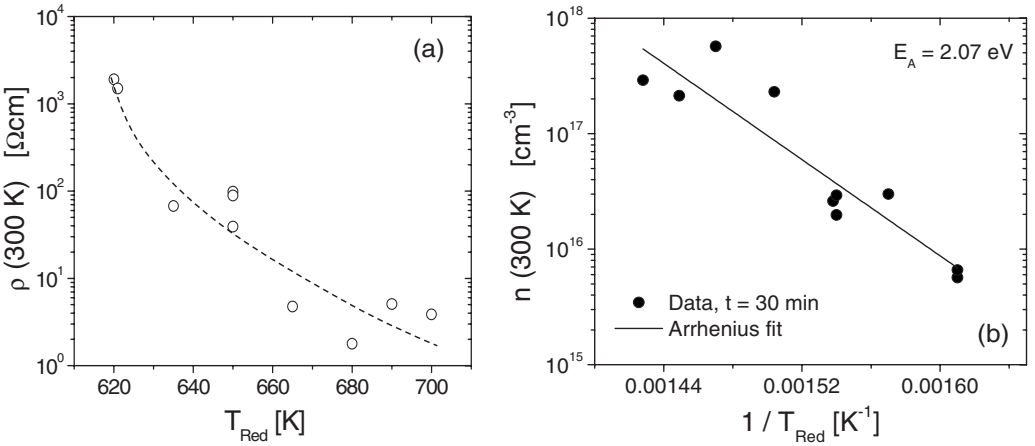

FIG. 1. (a) Dependence of the 300 K resistivity on reduction temperature. The reduction time was fixed at 30 min and the oxygen partial pressure was below 1×10^{-9} Torr. The dotted line is simply a guide to the eyes. (b) 300 K carrier density vs reciprocal reduction temperature for the same set of samples. The solid line is an Arrhenius fit with an activation energy of 2.07 eV. As for all data in this paper, the systematic errors on resistivity and Hall carrier density are estimated to be below 5–10 %, dependent on the overall magnitude of the resistivity.

substituted samples, in terms of both carrier density and resistivity.

Although some scatter is present in the data, there is a clear overall trend of increasing $n(300\ \mathrm{K})$ with increasing T_{Red}, as expected. This relationship was clarified by examining an additional set of samples where the UHV reduction time was held constant at 0.5 h. Figure 1(a) shows $\rho(300\ \mathrm{K})$ vs T_{Red} for these samples while Fig. 1(b) shows the equivalent carrier density plotted as $\log[n(300\ \mathrm{K})]$ vs $1/T_{Red}$. The data adhere reasonably well to an Arrhenius form with an activation energy of 2.1 eV. As discussed in prior work,[67–70] this can be rationalized in terms of simple thermodynamics where the reaction creating oxygen vacancies is written as $O_0 \rightarrow 1/2O_2 + V_O^{\cdot\cdot} + 2e'$, and $n(300\ \mathrm{K}) \approx 2[V_O^{\cdot\cdot}]$, due to the small value of E_D discussed above. According to Chan *et al.*,[67] this reaction is expected to dominate the reduction in $SrTiO_3$ at low P_{O2}. Our measured activation energy is in reasonable agreement with prior measurements on the (001) surface at similar temperature and P_{O_2} by Zhu *et al.*[68] but significantly lower than those obtained by Yamada and Miller.[69] However, in the latter case, the reduction was performed at much higher P_{O_2} and T_{Red} than most of our samples. Samples reduced at 1100 °C (see Table I), which have reduction conditions comparable to Yamada and Miller, do indeed have carrier densities in good agreement with that work.

Before proceeding to discuss macroscopic electronic-transport properties in more detail, it is important to discuss the issue of homogeneity of the reduction. Recent work has emphasized the complex nature of the reduction process in STO,[71–73] which was attributed to inhomogeneous oxygen-vacancy distributions[71,72] associated with the fast diffusion paths established at dislocations. Although it is clearly important to bear such issues in mind throughout this work, we would like to point out several factors pertaining to the homogeneity of the current distribution in our samples, and its impact on our conclusions: (i) the prior work on inhomogeneous reduction focused on samples reduced at fairly low temperatures. In our work, reduction temperatures up to 1100 °C have been employed, which significantly increases the bulk diffusion coefficients, potentially homogenizing the reduction process. (ii) As shown below, it is very significant that we observe quite consistent behavior in the temperature dependence of the resistivity for reduced and Nb-substituted samples with similar carrier density. *Unless the Nb doping process is also highly inhomogeneous, this clearly argues against strongly inhomogeneous conduction in the oxygen-deficient samples at these carrier densities.* (iii) In any case, the samples are clearly *macroscopically* homogeneous which is of primary importance for the proposed applications in thermometry and Hall sensing. This conclusion is drawn from analysis of the isotropy of the resistivity in van der Pauw measurements, in addition to the behavior of the Hall effect and MR as a function of orientation. Simple checks were also made to eliminate the possibility of purely surface currents, such as thickness scaling by polishing. Despite the above comments, it is nevertheless clear that additional future work comparing the transport properties of samples doped by various means would be beneficial. This would be particularly true for techniques capable of generating truly random dopant distributions (e.g., ion irradiation/implantation), at very low concentrations. This point will be returned to below.

The temperature dependence of ρ $(5<T<300\ \mathrm{K})$ of these 19 samples is shown in Fig. 2 along with T_{Red} (where relevant), N_{Nb} (where relevant), and $n(300\ \mathrm{K})$. A monotonic reduction in $\rho(300\ \mathrm{K})$ is observed with increasing n, with reasonably consistent $\rho(T)$ curves for reduced and Nb-substituted samples in the overlap region, as mentioned above. There are two main observations from Fig. 2 that require further discussion. First, at $T>75$ K, all curves exhibit a positive $d\rho/dT$ while at $T<75$ K, we observe a change in sign in $d\rho/dT$ with increasing n. Specifically, for n below about 2×10^{16} cm^{-3}, an insulatinglike $\rho(T)$ is observed below about 30 K (i.e., $d\rho/dT<0$) while for $n>2\times10^{16}$ cm^{-3}, a metallicklike $\rho(T)$ $(d\rho/dT>0)$ is observed. In addition, and as discussed below in more detail, the behavior of the low-temperature resistivity in this region is strange in that the low-T value of $d\rho/dT$ does not vary monotonically

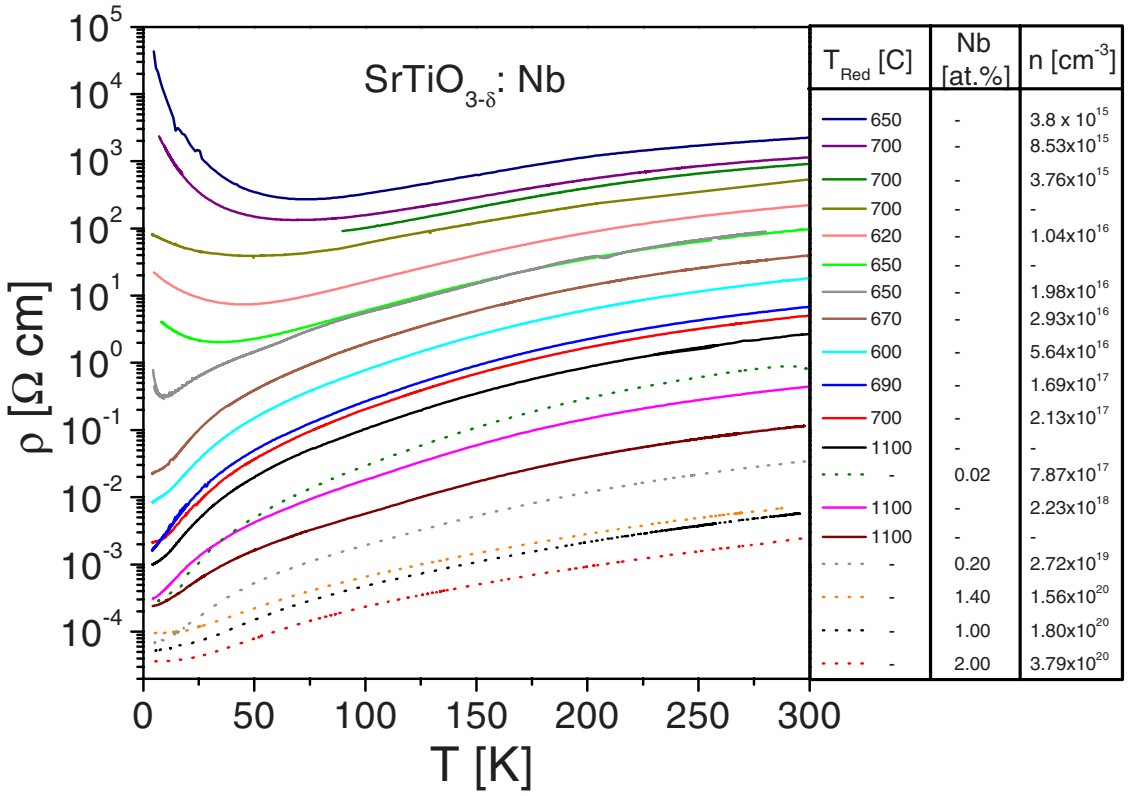

FIG. 2. (Color online) Temperature dependence of the resistivity (log scale) of 19 single crystals of $SrTiO_3$ doped by reduction (solid lines) or Nb substitution (dotted lines). The table displays the reduction temperature (where relevant), Nb doping concentration (where relevant), and 300 K Hall carrier density.

with n. Consider, for example, the $n=1.98\times10^{16}$ cm^{-3} data with anomalously large, and negative, $d\rho/dT$ at the lowest T. These two features clearly indicate a significant change in the character of the conduction at an electron density around 2×10^{16} cm^{-3}, which we designate n^*. This conclusion will be further reinforced by the $\mu(T)$ data presented below. The origin of the effect will be discussed in detail. The second striking feature of the data presented in Fig. 2 is the *magnitude* of $d\rho/dT$ in the range above 2×10^{16} carriers per cubic centimeter, where $d\rho/dT>0$ at all T. The resistivity is very strongly T dependent, with the residual resistivity ratio [RRR$=\rho$(300 K)$/\rho$(4.2 K)] reaching values as high as 3000. [Note that throughout this paper, we use the term "residual resistivity ratio" or "RRR" simply as a measure of ρ(300 K)$/\rho$(4.2 K), regardless of the regime in which transport occurs.] Such values are remarkably large and are normally only associated with high-purity metals, as opposed to relatively narrow bandwidth oxides. These two issues, i.e., the origin and consequences of the anomalously large $d\rho/dT$ in the metallic region, and the origin of the change in character of the transport around 2×10^{16} cm^{-3} are now discussed in detail.

The origin of the anomalously large positive $d\rho/dT$ is clarified by the data of Fig. 3(a) showing the T dependence of the Hall carrier density ($n=1/|R_He|$) in 11 representative samples. The most noteworthy feature is obviously the T *independence* of n, which, as discussed in Sec. I, can be interpreted in terms of the existence of small E_D due to the large ε_r of the paraelectric host. Although such effects were observed in STO crystals in several early studies,[32,35,38,41] it is important to note that in those earlier cases, T independence of R_H occurred only in heavily doped samples prepared either by Nb substitution or high-temperature reduction. More lightly doped samples (below 10^{17}–10^{18} cm^{-3}) consistently exhibited carrier freeze-out effects with characteristic activation energies of 35–100 meV, which were naturally interpreted in terms of nonhydrogenic "deep" levels.[32,35,38,41] It is therefore quite significant that the samples studied in this work exhibit no such carrier freeze-out effects down to n(300 K) at least as low as 4×10^{15} cm^{-3}. It should be emphasized that this is almost three orders of magnitude lower than samples exhibiting freeze-out in early work. Given the demonstration by Lee *et al.*[32] that high-T preannealing eliminates freeze-out effects in low-n samples, it is likely that the absence of these effects in our samples is due to the 1700 °C postgrowth annealing step. Future work to elucidate the relevant defect physics would be beneficial. $\mu(T)$ is shown for the same 11 samples in Fig. 3(b). The Hall mobility is strongly T dependent, increasing from 9 to 22 000 cm^2 V^{-1} s^{-1} on cooling from 280 to 7 K for $n=8\times10^{17}$ cm^{-3}, for example. All samples with $n>2\times10^{16}$ cm^{-3} exhibit monotonically decreasing μ with increasing T, following $\mu\propto T^{-m}$ at $T>100$ K, with m values in the range 2.8–3.2, similar to prior work.[32,35,38,42] The different behavior found at lower n will be discussed later. The high-n behavior is *qualitatively* consistent with scattering from optical phonons in this polar crystal, although, as discussed in Sec. I, we are not aware of any completely suc-

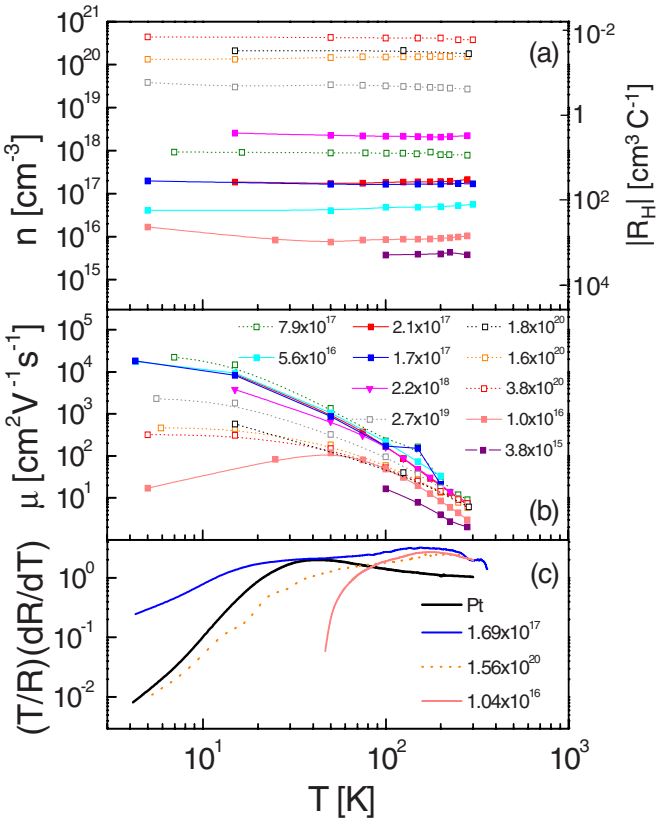

FIG. 3. (Color online) Temperature dependence (log-log scale) of (a) the Hall carrier density (the magnitude of the Hall coefficient is shown on the right axis), (b) the Hall mobility, and (c) the dimensionless temperature sensitivity $[(T/R)(dR/dT)]$ of multiple $SrTiO_3$ single crystals doped by reduction (solid points) or Nb substitution (open points). In (b) and (c), the curves are labeled with the 300 K Hall carrier density. In (c), the heavy line is a comparison to our data taken on a standard Pt thermometer (Ref. 95). The color scheme used here is identical to that employed in Fig. 2, to facilitate identification of the samples.

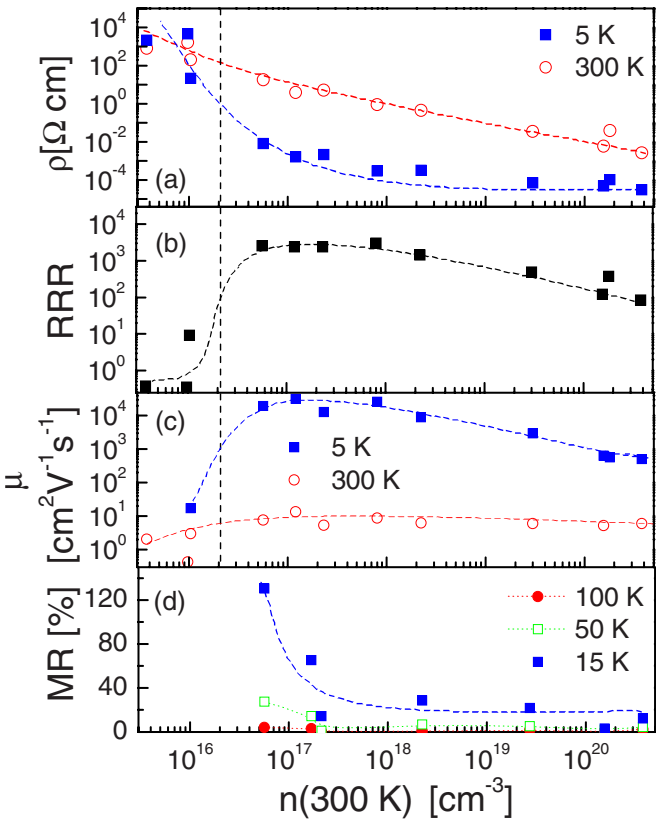

FIG. 4. (Color online) 300 K Hall carrier density dependence of (a) the resistivity, (b) the residual resistivity ratio [RRR $=\rho(300\ \mathrm{K})/\rho(4.2\ \mathrm{K})$], (c) the Hall mobility, and (d) the 9 T magnetoresistance $\{\mathrm{MR}=[\rho(9\ \mathrm{T})-\rho(0)]/\rho(0)\}$. The vertical dotted line marks the carrier density, $n^*=2\times10^{16}$ cm^{-3}. The dotted lines are simply guides to the eyes.

cessful quantitative modeling of $\mu(T)$. The importance of soft transverse-optical modes has been established however.[54,55] Naively, the strong temperature dependence of $\mu(T)$ can be viewed as being simply related to the high ε_r at low T, which guarantees effective screening of the ionized impurity scattering centers. However, as discussed above, the appropriateness of the hydrogenic picture for materials with nonlinear dielectric response has been questioned, and it may be that the temperature dependence of the nonlinearity is important.[56] In any case, the data on $n(T)$ in Fig. 3(a) and $\mu(T)$ in Fig. 3(b) now provide a clear picture of the origin of the large RRR and $d\rho/dT$ values shown in Fig. 2. Quite simply, the paraelectric host results in a large, strongly T dependent, $\varepsilon_r(T)$ giving rise to low E_D, the absence of carrier freeze-out, and temperature-independent n. At the same time, the mobility increases rapidly on cooling due to optical phonon scattering. The resistivity $[\rho(T)=1/n(T)e\mu(T)]$ thus exhibits a metalliclike T dependence with unusually large $d\rho/dT$, hence explaining the high RRR values. Later in the paper, we will discuss potential applications of this material based on the unusually large $d\rho/dT$.

We now turn to the second important issue arising from examination of the data of Fig. 2, i.e., the distinct change in the character of the conduction near $n^*=2\times10^{16}$ cm^{-3}, where the low-T sign of $d\rho/dT$ changes. The change in character of the transport is further illustrated by the data of Figs. 4(a) and 4(b) where ρ at 5 and 300 K, and the RRR, are plotted as a function of n. The carrier density 2×10^{16} cm^{-3} is shown as a vertical dotted line and it is clearly seen that the low-T resistivity increases quickly below this point, leading to a sharp decrease in RRR. Given that this change in character of the transport properties involves both a rapid increase in low-T resistivity and a change in sign of $d\rho/dT$, it is natural to consider the possibility of a doping-controlled $T=0$ MIT. In this context, the central issue is the existence (or otherwise) of nonzero conductivity in the zero-temperature limit. It is therefore interesting to replot the data of Fig. 2 as $\sigma(T)$ $[=1/\rho(T)]$, focusing on the low-T region. This is done in Fig. 5 which plots both $\rho(T)$ [Fig. 5(a)] and $\sigma(T)$ [Fig. 5(b)] in the region below 100 K. The most remarkable aspect of these data is the apparent observation of finite $\sigma(T\rightarrow0)$ for even the lowest carrier density samples. A more accurate assessment clearly requires measurements to lower T. For this reason, additional transport measurements down to 0.39 K were made on five samples $[n(300\ \mathrm{K})=8.5\times10^{15}, 2.0\times10^{16}, 2.9\times10^{16}, 1.7\times10^{17}$, and

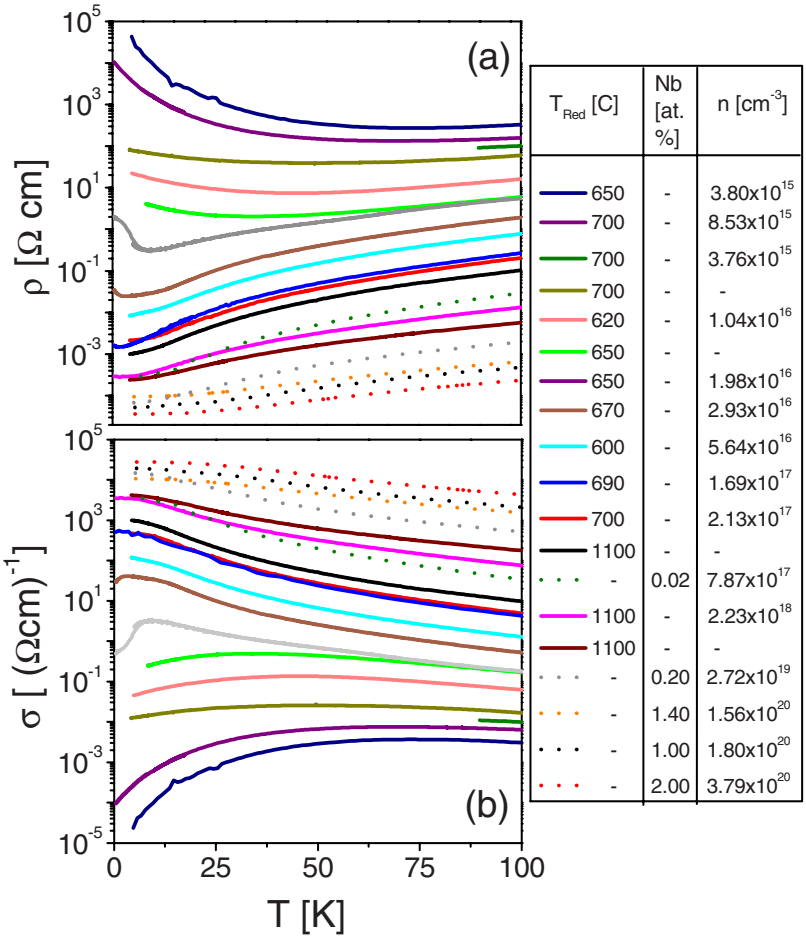

FIG. 5. (Color online) Temperature dependence of the (a) resistivity and (b) conductivity (on log-linear scales), for the same samples shown in Fig. 2, in the region below 100 K. Five samples were measured below 1 K, with 300 K carrier densities of 8.5×10^{15}, 2×10^{16}, 2.9×10^{16}, 1.7×10^{17}, and 2.2×10^{18} cm^{-3}. The color scheme used here is identical to that employed in Fig. 2, to facilitate identification of the samples.

2.2×10^{18} cm^{-3}], selected to be representative of the whole doping range covered in this study. The data are included in Figs. 5(a) and 5(b), and provide further confirmation of nonzero $\sigma(T\rightarrow0)$ down to very low carrier density [consider, for example, the $n(300\ \mathrm{K})=8.5\times10^{15}$ cm^{-3} sample]. This point is further clarified by Fig. 6 which plots $\sigma(T)$ down to ^{3}He temperatures, on a linear-linear scale, for two representative samples; one with $n(300\ \mathrm{K})=8.5\times10^{15}$ cm^{-3} (main panel) and the other with $n(300\ \mathrm{K})=2.9\times10^{16}$ cm^{-3} (inset). In both cases, $\sigma(T\rightarrow0)$ is clearly nonzero, confirming metallic behavior down to at least 8.5×10^{15} cm^{-3}.

The conclusion of metallic transport in these samples is further strengthened by a quantitative analysis of $\sigma(T)$. Specifically, it is well known from prior work on doped semiconductors[74–76] (as well as many other classes of materials) that in the weakly localized regime on the metallic side of the MIT, the T dependence of σ is provided by quantum corrections to $\sigma(T=0)$.[77–79] The conductivity is expected to take the form,

$$\sigma(n,T)=\sigma(n,T=0)+m(n)T^{1/2}+B(n)T^{p/2}, \qquad (2)$$

where m and B are constants for a given carrier density.[74–79] The $m(n)T^{1/2}$ term arises due to electron-electron interaction effects in the presence of disorder.[74–79] Simply, this can be viewed as arising from the perturbation in the density of states (DOS) at the Fermi level (E_F) due to electron-electron interactions, i.e., the "remnant" of the soft gap in the DOS at E_F on the insulating side of the MIT that gives rise to Efros-Shklovskii variable-range hopping (Ref. 80). The $B(n)T^{p/2}$ term on the other hand, is due to weak localization,[74–79] i.e., the partial destructive interference of electron wave functions that is destroyed by application of a magnetic field leading to the well-studied negative MR effects.[81] Within this framework, the relaxation time of the dominant dephasing process is expected to follow $1/\tau_\phi\propto T^p$, thus defining the constant p in Eq. (2).[74–79] Different scattering mechanisms result in different values of p, e.g., $p=3$ for electron-phonon scattering and $p=2$ and 3/2 for electron-electron scattering in the clean and dirty limits, respectively.[74–79] Data on the four samples measured below 4.2 K that could reasonably be expected to be in the weakly localized regime (i.e., not the $n=2.2\times10^{18}$ cm^{-3} sample with a low-temperature resistivity of order 300 $\mu\,\Omega$ cm) were initially fit with p as a free parameter, providing p values close to 3 in all cases. In subsequent fitting, p was thus constrained at exactly 3 and $\sigma(T=0)$, m, and B were allowed to vary. As demonstrated by the fits

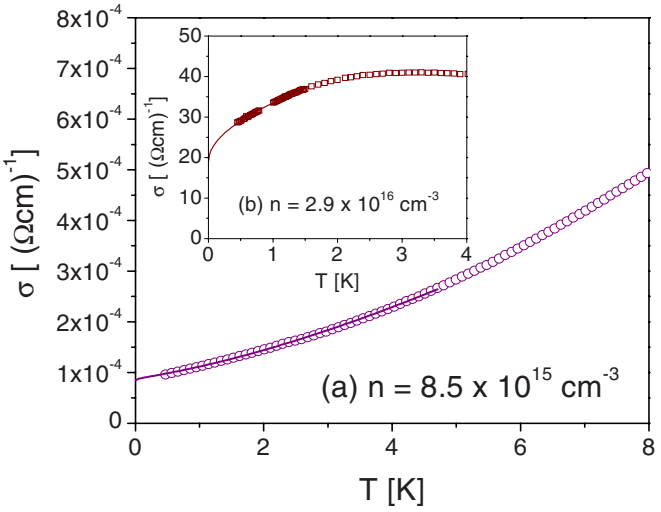

FIG. 6. (Color online) Temperature dependence of the low-temperature conductivity (linear-linear scale) of (a) an $n=8.5\times10^{15}$ cm^{-3} sample, and (b) an $n=2.9\times10^{16}$ cm^{-3} sample. The solid lines are fits to Eq. (2), with (a) $\sigma_0=8.5\times10^{-5}$ $(\Omega\ \mathrm{cm})^{-1}$, $m=1.2\times10^{-5}$ $(\Omega\ \mathrm{cm\ K}^{1/2})^{-1}$, and $B=1.5\times10^{-5}$ $(\Omega\ \mathrm{cm\ K}^{3/2})^{-1}$, and (b) $\sigma_0=18.9$ $(\Omega\ \mathrm{cm})^{-1}$, $m=14$ $(\Omega\ \mathrm{cm\ K}^{1/2})^{-1}$, and $B=0.5$ $(\Omega\ \mathrm{cm\ K}^{3/2})^{-1}$. Equivalent fits to the $n=1.7\times10^{17}$ cm^{-3} sample gave $\sigma_0=523$ $(\Omega\ \mathrm{cm})^{-1}$, $m=30$ $(\Omega\ \mathrm{cm\ K}^{1/2})^{-1}$ and $B=-10$ $(\Omega\ \mathrm{cm\ K}^{3/2})^{-1}$ while the $n=1.98\times10^{16}$ cm^{-3} sample gave $\sigma_0=2.6$ $(\Omega\ \mathrm{cm})^{-1}$, $m=-0.9$ $(\Omega\ \mathrm{cm\ K}^{1/2})^{-1}$, and $B=0.1$ $(\Omega\ \mathrm{cm\ K}^{3/2})^{-1}$. Note the change in sign in m for the sample with $n\approx n^*$, and the general observation that the electron-electron interaction term dominates the weak-localization term.

shown in Fig. 6, Eq. (2) with $p=3$ is indeed a good description of our data at the lowest T. Most importantly, and in agreement with our earlier qualitative conclusion, the $\sigma(T=0)$ values were finite for all samples. As an example of typical extracted parameters the sample with $n(300\ \mathrm{K})=2.9\times10^{16}$ cm^{-3} gives $m=14$ $(\Omega\ \mathrm{cm\ K}^{1/2})^{-1}$ and $B=0.5$ $(\Omega\ \mathrm{cm\ K}^{3/2})^{-1}$, comparable to conventional semiconductors with similar conductivity values.[74–76] The fitting parameters for all samples are provided in the caption to Fig. 6. The factor m in Eq. (2) is given by $m=\alpha[4/3-(3/2)(\gamma F_\sigma)]$, where α is simply related to the diffusion coefficient, and the factor γF_σ is related to the Fermi-liquid interaction parameter.[77] The two terms are due to exchange and Hartree-type effects, respectively, and it is important to note that the anticipated high screening in STO would apparently only influence the competition between theses two terms, via the obvious screening length dependence of F_σ. In this context, it is worthwhile pointing out (see caption of Fig. 6 for more details) that we typically find positive m values. In summary, the data of Figs. 5 and 6 demonstrate quite clearly that these doped $SrTiO_3$ samples are metallic conductors down to carrier densities as low as 8.5×10^{15} cm^{-3}, possibly even lower. To place this in context, the critical carrier density for the MIT (n_c) in most semiconductors is orders of magnitude higher than this. Ge, for example, has $n_c\approx3\times10^{17}$ cm^{-3} while for Si $n_c\approx5\times10^{18}$ cm^{-3}.[82,83]

The surprisingly low n_c value that we deduce must be present in doped $SrTiO_3$ can be viewed as another consequence of the paraelectric nature of the host. As can be seen from Eq. (1), in the hydrogenic picture, the large, highly T-dependent $\varepsilon_r(T)$ gives rise to a large, strongly T-dependent Bohr radius for the donor impurities. Simple calculations based on the best available estimates for m_e^*,[38] and the measured $\varepsilon_r(T)$,[2–5] yield $a_B\approx200$ nm at 300 K, increasing dramatically to ≈10 μm at liquid-helium temperatures. These very large estimated a_B values imply the onset of significant overlap of donor atom wave functions at very low carrier densities. Employing the Mott criterion, $n_c^{1/3}a_B\approx0.26$, which has been extraordinarily successful for a wide variety of systems, over at least an 8 order of magnitude range of n_c,[83] we obtain an n_c that is strongly T-dependent [due to $\varepsilon_r(T)$], reaching values as low as 1×10^{13} cm^{-3} at low T, i.e., many orders of magnitude lower than conventional semiconductors. It is worth pointing out that ε_r becomes independent of T below about 30 K in $SrTiO_3$ meaning that n_c does reach a limiting value in the low-T region of interest. Based on this estimate of n_c, the observation of metallic conduction down to at least 8.5×10^{15} cm^{-3} is understood. As discussed above, it is also important to consider the possibility that the hydrogenic picture is inapplicable.[56] In this situation, according to Epifanov and Levanyuk, the donor ionization energy is likely to be weakly T dependent.[56] In any case, it is clear from the observation of metallic transport down to such low carrier densities that the donor radii are unusually large. Clearly, measurements to lower n to properly probe the MIT in STO would be very interesting but this would require a means to control the doping at very low carrier density. We are aware of only one study where such low carrier density was achieved by reduction but very low-T measurements were not reported.[54] Ion implantation, ion irradiation,[84] and electrostatic gating[61,85] are alternative possibilities for such a study, as is the use of the low-T positive MR discussed below. As discussed above, photodoping has been used to probe the extreme quantum limit of magnetotransport in this material[63] and can also be used to probe the MIT. In fact, Kozuka *et al.*[64] have used the wavelength dependence of the optical penetration depth in as an elegant means to tune the effective dimensionality and study the MIT. They observed a 2D MIT around 5×10^{11} cm^{-2} but found no such transition in the three-dimensional (3D) case down to electron densities as low as 10^{14} cm^{-3}. This observation, in addition to their interpretation in terms of the Mott criterion using the large low temperature ε_r, is completely consistent with our observations in doped bulk crystals.

It is important at this point to consider the validity of the process of using the undoped static dielectric response [i.e., the $\varepsilon_r(T)$ of stoichiometric $SrTiO_3$] in calculations of n_c. In particular, if ε_r were suppressed with doping we would underestimate n_c. There are at least three arguments that this is unlikely. First, the impurity concentrations relevant to the discussion here are sufficiently small (10^{13}–10^{20} cm^{-3}) that a significant modification of the lattice response is unlikely. Second, in conventional semiconductor hosts the doping process actually leads to an enhancement of ε_r due to the contribution from the doped carriers. This effect involves a divergence in $\varepsilon_r(n)$ as the MIT is approached and the localization length diverges.[83] Finally, although the available data are not entirely complete, some measurements of ε_r as a function of impurity concentration have been made.[34,86,87]

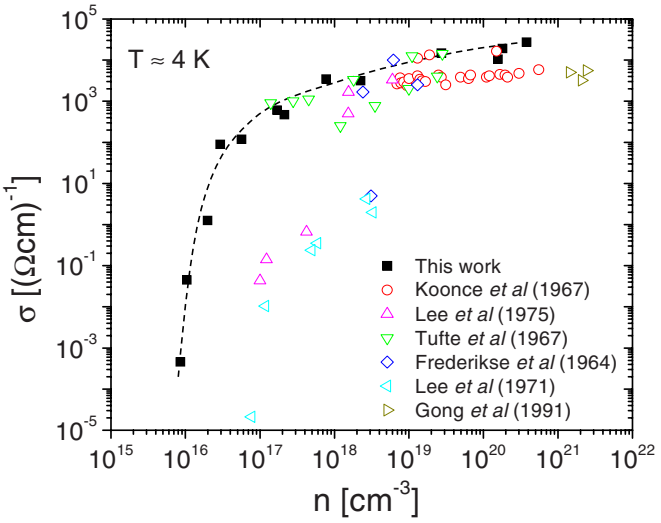

FIG. 7. (Color online) Log-log plot of the low-temperature (4–5 K) conductivity vs carrier density [at 300 K with the exception of Koonce *et al.* (Ref. 54)] compiled from this work, and six prior publications (Refs. 31, 34, 37, 41, 54, and 66). The dotted line is a guide to the eyes.

Often a nonmonotonic dependence is observed, with ε_r first increasing to a maximum, then decreasing at much higher concentrations (above ~1 at. %).[34,86,87] Of most relevance to the current discussion, this behavior has been observed for both Nb (Ref. 88) and La (Ref. 34) impurities, both of which are dopants in STO. At the impurity concentrations of relevance to the current paper ε_r is actually *increased* over the undoped value.[34,88] It should be noted that this is not a general phenomenon and other dopants may behave differently.

The final point to be made about the rather low upper bound for n_c we obtain from our data is that it is in contrast to the conclusions of some prior work.[44,59] These earlier conclusions were arrived at based on examination of low (^{4}He) temperature $\sigma(n)$ plots compiled from multiple studies, as opposed to more direct methods based on estimation of $\sigma(T\rightarrow 0)$ from very low-T measurements, as shown in this paper. Figure 7 shows such a compilation of $\sigma(n)$ data. Following Calvani *et al.*,[59] the σ values are taken from this work in addition to six prior publications, and are measured in the range 4–5 K while the n values are at room temperature. Although the data from prior work exhibit considerable scatter, there is a several order of magnitude increase in σ in the 10^{18} cm^{-3} range, which led to the conclusion in prior studies that an MIT takes place in this region. Our own data (solid points in Fig. 7), which exhibit a very clear trend with n(300 K), show considerably higher conductivity at a given room-temperature carrier density. This is likely related to the absence of carrier freeze-out effects in the current study, as discussed above. In any case, the important point to be taken from Fig. 7 is that the MIT is located at much lower n than previously concluded. Again, it must be stressed that all of the samples shown in this figure exhibit finite $\sigma(T\rightarrow 0)$. As discussed above, our observation of metallic conductivity to such low carrier densities in these bulk, doped samples is consistent with the 3D photodoping results of Kozuka *et al.*[64]

Having established that all samples studied in this work are on the metallic side of the MIT, and that the unusual change in character of the transport at $n^*\approx 2\times 10^{16}$ cm^{-3} cannot therefore be associated with an MIT, alternative possibilities must be considered. The form of $\mu(T)$ in this carrier density region provides additional valuable information. In particular, inspection of Fig. 3(b) reveals that samples with $n<n^*$ exhibit distinctly lower μ than higher-n samples, with a turnover below about 50 K where μ begins to decrease with decreasing T, as opposed to saturating at a T-independent value. In this region (5 to 50 K), the mobility roughly follows a power-law form, $\mu\propto T^{\alpha}$, with $\alpha\approx 0.7$. This distinctly different mobility behavior is also evident when examining the n dependence, as shown in Fig. 4(c), where it can be seen that μ decreases rapidly with decreasing n below 2×10^{16} cm^{-3}, resulting in a peak in $\mu(n)$ at low T. This feature has in fact been observed in multiple prior studies, as pointed out by Ohtomo *et al.*[60] who presented a composite plot from earlier work on bulk samples. This conclusion does not therefore rest on the single low n point in Figs. 3(b) and 4(b). It remains however to be explained. Clearly this behavior is *not* due to ionized impurity scattering as the anomalous behavior occurs at the *lowest* n. The fact that the samples with $n<n^*$ are synthesized at the lowest T_{Red} values (620–700 °C, Table I) suggests that it is possible that this behavior has a structural origin, e.g., decreased μ arising from increased defect density due to defects that are not "annealed out" over the course of the reduction process at such low T_{Red} values.[42] Prior reports of "self-healing" during reduction[71] are clearly relevant here. Although this mechanism could explain the global crossover from positive to negative $d\rho/dT$ with decreasing n, it is not clear how it could account for the nonmonotonic dependence of low-temperature $d\rho/dT$ on n. Additionally, the specific possibility of increased scattering from dislocations at low T_{Red} was explicitly considered by Lee *et al.*,[42] who concluded, based on data from several prior studies,[89–92] that this effect should be negligible. Finally, it should be noted that these crystals were subject to a 48 h postgrowth annealing process at 1700 °C, decreasing the likelihood that a significant amount of defect annealing occurs during reduction at 620–700 °C.

Alternatively, the change in character of the transport at $n=n^*$ may have an electronic origin. The most significant observation in this regard is the nonmonotonic dependence of the low-T $d\rho/dT$ with n. As touched upon earlier, close examination of Figs. 2 and 5 show that the smooth evolution from negative to positive low-T $d\rho/dT$ with increasing n is interrupted in the region $1.04\times 10^{16}<n<2.93\times 10^{16}$ cm^{-3}, which corresponds to low T resistivities from 2×10^{-2} to 2×10^{1} Ω cm. In this region, where μ is lowest and increases with T [see Figs. 3(b) and 4(c)], $d\rho/dT$ takes anomalously large negative values, best exemplified by the $n=1.98\times 10^{16}$ cm^{-3} data, which were acquired down to 0.4 K (Fig. 5). This is illustrated more clearly in Fig. 8 which plots $[(1/\rho)(d\rho/dT)]$ at 6 K as a function of ρ(300 K), highlighting the nonmonotonic behavior in the vicinity of n^*. Although the $n=1.98\times 10^{16}$ cm^{-3} sample has by far the highest negative $d\rho/dT$ value, it can be clearly seen that adjacent points confirm the trend, showing a dip around n^*. In essence, in a narrow region of carrier density around n^*, the high-T resistivity behaves normally whereas the low-T resistivity appears to reflect some additional localization mecha-

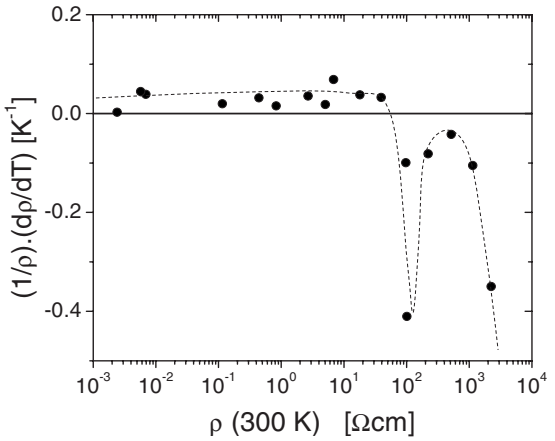

FIG. 8. Linear-log plot of $(1/\rho).(d\rho/dT)$ at 6 K vs the 300 K resistivity showing the strong negative peak in $d\rho/dT$ in the region close to the sign reversal in $d\rho/dT$. The dashed line is a guide to the eyes.

nism which disappears as n is increased or decreased. One simple possibility, which provides qualitative explanations for all observed phenomena, is a model based on the occurrence of a transition from impurity-band (IB) to conduction-band (CB) transport with increasing n. This is based on the well-known concept that sufficiently heavy doping of semiconductors leads to the individual donor levels broadening into an impurity band due to the effects of Coulombic interactions of randomly positioned donors/compensating defects, as well as polarization of neutral donors by ionized neighbors.[80] The result is an impurity-band density of states $[D_{\mathrm{IB}}(E)]$ with a finite width, Δ, centered on the original donor-level ionization energy, E_D. In our case, the vanishing E_D (which centers the IB on the CB edge, E_C) implies that the $D_{\mathrm{IB}}(E)$ should overlap with the CB DOS, $[D_{\mathrm{CB}}(E)]$ giving a total DOS, $D_{TOT}(E)$, that is nonmonotonic with E, having a local minimum at some energy E^*, i.e., a "neck" in the density of states as a function of energy. At $n<n_c$ (i.e., lower carrier densities than we are able to achieve here), the Fermi energy, $E_F(n)$, lies below the mobility edge, E_μ, in the lower tail of the IB, the donor wave functions are localized, and the system is insulating $[\sigma(T\rightarrow 0)=0]$. As n is increased to n_c and $E_F(n)$ reaches E_μ, the wave functions become delocalized, metallic transport emerges, and $\sigma(T\rightarrow 0)$ becomes finite. The lowest carrier densities in this study ($\sim 10^{15}$ cm^{-3}) are already above this point. Further increases in $E_F(n)$ lead to improved conductivity and mobility up to the point where E_F approaches E^*. At this point, E_F is located in the local minimum in $D_{TOT}(E)$ where the IB and CB merge. We propose that this corresponds to the n^* determined from our data, i.e., $E_F(n=n^*)=E^*$. As n increases beyond this point, $E_F(n)$ moves into the CB and a transition from IB to CB conduction occurs. This simple model can explain, at least qualitatively, all key features of our data. Specifically, the sharp increase in $\rho(5\ \mathrm{K})$, the accompanying decrease in RRR and low temperature μ [Figs. 4(a)–4(c)], and the change in sign in the low temperature $d\rho/dT$ (Fig. 2) are all consequences of the crossover from CB to IB conduction as n is decreased. Close to the crossover point, when $n\approx n^*$, the large, negative, $d\rho/dT$ values at sufficiently low T then occur due to the anomalously low $D_{TOT}(E)$, explaining the nonmonotonic behavior illustrated in Fig. 8. It is worth noting that the importance of IB conduction has also been emphasized in other low-n_c semiconductors, n-type InSb being an excellent example.[93,94] This material has $n_c\approx 10^{14}$ cm^{-3}, similar to our estimates for STO, although in this case, the low-n_c value is driven more by the unusually small electron effective mass $(m_e^*/m_e=0.015)$ than a large ε_r.[95] Of primary importance for this discussion, it has been pointed out that for such IB conduction in InSb a low mobility increasing as $T^{1/2}$ is expected.[94] This is quite similar to what we observe in Fig. 3(b) when $n<n^*$, i.e., μ increasing as $T^{0.7}$, adding further weight to our arguments.

Although this picture is qualitatively consistent with the observed phenomena, it is worthwhile to discuss potential issues with its applicability. First and foremost it must be acknowledged that the width of the IB, Δ, is in fact a function of n.[80] If the n_c in STO is really as low as the 10^{13} cm^{-3} value from simple estimates, it is possible that by carrier densities of order 10^{16} cm^{-3} the IB would have completely merged with the CB, i.e., no neck would remain in the DOS as a function of energy. It is important to point out however that the lowest densities probed here are around 3×10^{15} cm^{-3}, considerably above the 10^{13} cm^{-3} estimate from the Mott criterion. It is thus possible that n_c is significantly larger than the simple prediction, meaning that we are probing n/n_c values less than we expect. In this regard, it should be mentioned that simple estimates of the minimum metallic conductivity using $\sigma_{\mathrm{min}}=0.03e^2/\hbar a_c$, where $a_c\approx n_c^{-1/3}$,[79] yield values around 0.2 $(\Omega\ \mathrm{cm})^{-1}$ for STO. Although the existence of a discontinuous MIT with a true σ_{min} is no longer believed to occur (due to the success of the scaling theory of electron localization where the transition is continuous[77,80,83]), it is nevertheless true that in many systems the MIT occurs quite close to σ_{min}.[83] If this were the case in STO then it could be concluded from the above estimate of 0.2 $(\Omega\ \mathrm{cm})^{-1}$, in conjunction with the data of Fig. 7, that the lowest densities probed in this work (around 10^{15} cm^{-3}) are indeed quite close to the MIT. Further studies, to lower n, will be required to settle this issue. As mentioned above, even photodoping experiments[64] have not yet reached low enough n to determine the 3D n_c. There are also a number of reports, from both theoretical[96] and experimental perspectives,[97] of the possibility of a distinct IB persisting far above n_c. This would indicate that the model we present here is plausible. It should also be noted that the picture presented above simply requires some structure in the CB that produces a region with an anomalously low DOS. It is possible that mechanisms other than a merged IB/CB could generate such a feature. Most importantly, we would prefer to make a quantitative test of this proposed model to check whether agreement with experiment can be obtained for reasonable parameters. Consider, for example, a crude model where $D_{TOT}(E)$ is taken as the sum of a simple 3D free-electron-like CB density of states, $D_{\mathrm{CB}}(E)$, and an IB density of states with a Gaussian shape, i.e. $D_{\mathrm{IB}}(E)=D_{\mathrm{IB}}^0\exp -(E^2/2\Delta^2)$, where D_{IB}^0 is the maximum IB density of states. (Note that we are taking the CB edge as the zero of energy). Integrating over $D_{TOT}(E)$ leads to

$$n(E_F) = \frac{1}{3\pi^2}\left(\frac{2m_e^* E_F}{\hbar^2}\right)^{3/2} + D_{\mathrm{IB}}^0 \Delta\sqrt{2\pi}\left[\frac{1}{2} + \frac{1}{2}\mathrm{erf}\left(\frac{E_F}{\sqrt{2}\Delta}\right)\right], \tag{3}$$

where $\mathrm{erf}(x)$ is the Gauss error function. Putting $\partial D_{TOT}(E)/\partial E = 0$ then allows us to derive an expression involving the energy (E^*) at which the local minimum in the DOS occurs,

$$(E^*)^{1/2}\exp\left[\frac{-(E^*)^2}{2\Delta^2}\right] = \frac{\Delta}{2\sqrt{2}\pi^2 D_{\mathrm{IB}}^0}\left(\frac{2m_e^*}{\hbar^2}\right)^{3/2}. \tag{4}$$

In principle, then, given values for Δ and D_{IB}^0, E^* can then be computed and inserted into the expression for n^* obtained from Eq. (3), i.e.,

$$n^* = n(E_F = E^*) = \frac{1}{3\pi^2}\left(\frac{2m_e^* E^*}{\hbar^2}\right)^{3/2} + D_{\mathrm{IB}}^0 \Delta\sqrt{2\pi}\left[\frac{1}{2} + \frac{1}{2}\mathrm{erf}\left(\frac{E^*}{\sqrt{2}\Delta}\right)\right] \tag{5}$$

enabling comparison to the experimentally determined n^* value. (Note that integration over $D_{\mathrm{IB}}(E)$ shows that the factor $D_{\mathrm{IB}}^0\Delta(2\pi)^{1/2}$, i.e., the prefactor in the second term, is simply N_{IB}, the number of states in the IB). The major issue is that estimation of n^* thus requires knowledge of both N_{IB} and Δ, neither of which are well known in our case. An accurate calculation would also require explicit consideration of the n dependence of Δ, taking into account the density of compensating centers, which is again unknown in this case. Having said this, rough estimates of the important parameters do yield physically reasonable values. For instance, reasoning that the minimum in $\rho(T)$ in the vicinity of n^* must occur roughly at E^*/k_B, i.e., the Fermi temperature at n^*, we obtain (from the 2×10^{16} cm^{-3} sample) $E^* \approx 0.8$ meV. Taking $\Delta \approx E^*$ (we use $E^* = \Delta/\sqrt{2}$ for convenience) gives $N_{\mathrm{IB}} \approx 4\times10^{17}$ cm^{-3} [from Eq. (4)] and subsequently $n^* \approx 5\times10^{17}$ [from Eq. (5)]. The order of magnitude disagreement with experiment (where $n^* \approx 2\times10^{16}$ cm^{-3}) is not unreasonable given the approximations made. A more accurate treatment would employ a physically reasonable form for the structure of the IB (with explicit density dependence), as is obtained from the Lifshitz model, for instance.[80] As a final note on this IB conduction model, we would like to point out that the picture proposed here is significantly different than the IB conduction model of Lee *et al.*[42] That model was constructed to explain experimental data showing carrier freeze-out effects in samples with n(300 K) as high as 8×10^{16} to 3×10^{18} cm^{-3}. In our case, carrier freeze-out effects are negligible, there is no evidence of nonhydrogenic deep levels, and we have clearly demonstrated that all samples are metallic. Moreover, in our case, we use the model not only to understand the abrupt changes in $\rho(5\ \mathrm{K})$, RRR, and low-T mobility with increasing n but also to explain the anomalous nonmonotonic behavior of the low-temperature $d\rho/dT$, which, to the best of our knowledge, has not been previously reported.

As a final remark on the transport properties of these doped STO samples, the investigated T range was extended to 20 mK for a single Nb-doped sample with $n(300\ \mathrm{K}) = 1.8\times10^{20}$ cm^{-3}, in order to determine the superconducting transition temperature, T_c. The resistivity data (not shown) reveal an onset T_c of 340 mK with a transition width of 90 mK. At 20 mK the critical field was found to be around 30 mT. The interesting feature of these results is that the T_c is significantly above the dome found in Ref. 58, and in fact lies quite close to the two outlying points in Ref. 58 at $n = 1.5\times10^{20}$ cm^{-3}, $T_c = 410$ mK and $n = 2.1\times10^{20}$ cm^{-3}, $T_c = 295$ mK. Clearly, future studies of $T_c(n)$ in heavily characterized samples would be beneficial.

IV. POTENTIAL APPLICATIONS

We would like to advance several potential applications of doped STO based on the data presented above. The first of these exploits the very large values of $d\rho/dT$ and RRR reported in Figs. 2 and 4(b), which, as we have discussed in detail, arises due to the combined effects of the small E_D and highly T-dependent mobility. The RRR values reported in Fig. 4(b), (up to 3000), are in fact considerably greater than those found in the metals used in commercial metallic (i.e., $d\rho/dT > 0$) RTDs (resistance temperature detectors). Metallic RTDs based on materials such as Pt or RhFe are commonly employed in applications that require wide-range cryogenic/elevated temperature ranges, high-temperature sensitivity, and high repeatability.[98,99] In contrast to semiconductor (i.e., $d\rho/dT < 0$), RTDs (e.g., Ge, carbon-glass, Cernox, etc.), metallic RTDs are able to maintain high sensitivity over a wide T range. One of the limitations of such devices is the lower limit on the usable range (around 30 K for Pt) due to the rapidly diminishing $d\rho/dT$ as phonon excitation is diminished and the residual resistivity is approached.[98,99] Figure 3(c) shows a comparison of the dimensionless sensitivity, $S = (T/R)(dR/dT)$, of a standard Pt thermometer (model PT102, Lakeshore Cryotronics, Inc. [Ref. 100] and three samples of doped STO from this study ($n = 1\times10^{16}$, 1.7×10^{17}, and 1.6×10^{20} cm^{-3}). Remarkably, the $n = 1.7\times10^{17}$ cm^{-3} sample exhibits higher sensitivity than Pt over the entire range. This is particularly true at low T, where the dimensionless temperature sensitivity exceeds that of Pt by an order of magnitude, potentially expanding the usable range to liquid-helium temperatures and avoiding one of the major problems with Pt RTDs. It is important to stress that this high sensitivity is not restricted to a narrow doping range. Although it is immediately apparent from Fig. 3(c) that lower carrier densities provide inferior performance, Fig. 4(b) shows that RRR values in excess of 10^3 occur over a *two order of magnitude* doping range from 3×10^{16} to 2×10^{18} cm^{-3}.

Potential issues with these applications should be addressed. First, the absolute resistance values of bulk single-crystal samples are very low. Although this may not be an issue for certain high-sensitivity niche applications where appropriate measurement instrumentation is available, this is not appropriate for typical RTDs. It is anticipated that thin-film devices would be required to achieve reasonable resis-

tance values. Although this is beyond the scope of the current work it should be noted that a rapidly expanding literature exists on the growth and characterization of such doped STO films [e.g., Refs. 8, 17, 18, 60, and 62]. Additionally, although we have performed simple tests to confirm that the resistance values are robust to a few thermal cycles, long-term repeatability is yet to be assessed. The same is true of the upper T limit for these materials although initial experiments indicate time-independent resistivities to temperatures of order 350 K. Sensitivity to applied magnetic fields is also important. In order to make a preliminary assessment of this issue we made 9 T MR measurements on a subset of the samples in Fig. 2. All MR measurements were performed with the field perpendicular to the plane and it is important to acknowledge that alternative orientations may minimize field-induced temperature errors. As shown in Fig. 4(d), the MR values are small above 50 K at all doping values. Below this temperature significant positive MR effects are observed, becoming increasingly large with decreasing n. The MR is roughly parabolic with applied field, and increases quickly with decreasing T, i.e., it is qualitatively consistent with the positive MR effects observed in other degenerately doped semiconductors[75,93,97] near the MIT. It is worth noting that this provides a potential route to field tune the MIT from the metallic side in future work. Note that the MR effects are greatly diminished at $n > 2 \times 10^{17}$ cm^{-3}, even at low T. This is well within the range where the high RRR values are maintained [Fig. 4(b)], indicating that high sensitivity can be obtained in a carrier density regime where the MR effects are modest.

As a final note on potential applications based on the large $d\rho/dT$, we mention the possibility of using doped STO in thin-film microcalorimeters. Silicon-nitride-based devices manufactured using microfabrication techniques have been available for over a decade and can be used to measure the heat capacity of thin films and heterostructures deposited directly on these "calorimeters-on-a-chip."[101–107] Such devices enable the power of specific-heat measurements to be harnessed in thin-film samples. These devices have been used in studies of materials such as magnetic semiconductors,[103] giant magnetoresistive multilayers,[104] amorphous semiconductors,[105] etc. A serious limitation however is the need to deposit the materials under study directly on the amorphous nitride membranes. This is compatible with the study of amorphous or polycrystalline films but does not typically allow for study of epitaxial structures, where a single-crystal lattice-matched substrate is required. Thus, despite the success of heat-capacity measurements in elucidating the physics of complex oxides such as manganites, these measurements cannot be conducted on the epitaxial complex oxide heterostructures that currently attract such attention. Development of microcalorimeters using perovskite substrates would open up a number of new possibilities, and we propose that doped STO thin-film thermometers could be a key component of such devices, having epitaxial compatibility with the substrate and overlying film. Note that current devices resort to the use of multiple thin-film RTDs [e.g., Pt (Ref. 101) and a-Si:Nb (Ref. 106)] in order to adequately cover the required T range with sufficient sensitivity. As an additional advantage, the improved temperature sensitivity of doped STO films could enable the use of a single thermometer over a wide range, simplifying designs, minimizing the number of leads required, and reducing the overall lateral footprint[107] of the device.

The second area in which we propose potential applications could arise is Hall sensing. Hall-effect-based field sensors are used in a wide variety of applications including proximity sensors/switches, speed measurement, current sensing, and laboratory field sensing.[108] The appeal of doped STO for use in such devices is the existence of the large, temperature-independent Hall coefficient, due to the absence of carrier freeze-out to anomalously low n. The right axis of Fig. 3(a) shows the Hall coefficient ($R_H = 1/n|e|$) as a function of T for several samples, demonstrating temperature-independent R_H values in excess of 10^3 cm^3 C^{-1}. Although currently employed materials such as GaAs and InSb exhibit R_H values comparable to those shown here, the temperature independence in STO, which arises due to the small E_D, could offer an extended temperature range for industrial applications, or the advantage of near temperature independence to cryogenic temperatures in laboratory applications. Moreover, the work of Kholkin *et al.* reported R_H up to 10^6 cm^3 C^{-1} in lightly reduced STO.[54] It should be noted however that high sensitivities of doped STO sensors could likely only be exploited in current-biased sensors. In current biasing, the Hall voltage $V_H = R_H BI/t$, where B is the applied flux density, I is the bias current, and t is thickness. The sensitivity of current-biased thin-film sensors is thus directly limited by R_H. Typical sensitivity of commercial devices is in the millivolt per gauss range,[108] i.e., 10 V T^{-1}, which, based on the data of Fig. 3(a), could be achieved in doped STO with $n = 1 \times 10^{16}$ cm^{-3}, and $t = 1$ μm, for a bias current of 10 mA. Epitaxial thin films of doped STO could thus have significant application potential if low carrier densities can be reliably obtained. In a voltage-biased device however, $V_H = \mu VB$, where V is the bias voltage. Under these circumstances, the sensitivity is thus limited by the mobility, meaning that STO would only be competitive with materials such as InSb [room-temperature electron mobility of 78 000 cm^2 V^{-1} s^{-1} (Ref. 95)] and GaAs [8800 cm^2 V^{-1} s^{-1} (Ref. 95)] at low temperatures [see Fig. 3(b)].

V. SUMMARY

We have revisited the electronic transport in doped $SrTiO_3$, by examining a large set of n-type single crystals over a wider doping range than previously possible. We observed a temperature-independent Hall coefficient to very low carrier density, highly temperature-dependent resistivity and mobility, and a remarkably low upper bound for the critical carrier density for the metal-insulator transition. These phenomena are all consequences of the unusual dielectric response, which leads to vanishingly small donor ionization energies, the absence of carrier freeze-out, phonon-limited mobilities, and overlap of donor ion wave functions at unusually low densities. The result is an unusual high-mobility low carrier density metallic state. In addition, a distinct crossover in conduction mechanism occurs at a carrier

density around 2×10^{16} cm^{-3}, which we interpret in terms of a transition from impurity-band to conduction-band transport. In short, we have provided a basic framework for the understanding of the global transport properties of doped $SrTiO_3$. Based on these remarkable transport properties, we propose potential applications for doped $SrTiO_3$ in resistive thermometry and Hall sensing.

ACKNOWLEDGMENTS

Work supported by NSF under Grant No. DMR-0804432. We are indebted to Yen-Hsiang Lin and Allen Goldman for measurements below 300 mK, and M. Sharma for some of the x-ray diffraction. We acknowledge insightful discussions with B. Shklovskii, J. Mitchell, and B. Zink.

*Corresponding author; leighton@umn.edu

[1] J. B. Goodenough, *Localized to Itinerant Electronic Transitions in Perovskite Oxides*, Structure and Bonding Vol. 98 (Springer, New York, 2001).
[2] J. H. Barrett, Phys. Rev. **86**, 118 (1952).
[3] K. A. Müller and H. Burkard, Phys. Rev. B **19**, 3593 (1979).
[4] J. Hemberger, P. Lunkenheimer, R. Viana, R. Bohmer, and A. Loidl, Phys. Rev. B **52**, 13159 (1995).
[5] H. Uwe and T. Sakudo, Phys. Rev. B **13**, 271 (1976).
[6] H.-M. Christen, J. Mannhart, E. J. Williams, and Ch. Gerber, Phys. Rev. B **49**, 12095 (1994).
[7] C. S. Hwang, S. O. Park, C. S. Kang, H.-J. Cho, H.-K. Kang, S. T. Ahn, and M. Y. Lee, Jpn. J. Appl. Phys. **34**, 5178 (1995).
[8] S. Gopalan, C.-H. Wong, V. Balu, J.-H. Lee, J. H. Han, R. Mohammedali, and J. C. Lee, Appl. Phys. Lett. **75**, 2123 (1999).
[9] K. Morito, T. Suzuki, S. Sekiguchi, H. Okushu, and M. Fujimoto, Jpn. J. Appl. Phys. **39**, 166 (2000).
[10] D. Fuchs, C. W. Schneider, R. Schneider, and H. Rietschel, J. Appl. Phys. **85**, 7362 (1999).
[11] R. Ramesh and D. G. Schlom, MRS Bull. **33**, 1006 (2008).
[12] J. Heber, Nature (London) **459**, 28 (2009).
[13] M. Kawasaki, K. Takahashi, T. Maeda, R. Tsuchiya, M. Shinohara, O. Ishiyama, T. Yonezawa, M. Yoshimoto, and H. Koinuma, Science **266**, 1540 (1994).
[14] M. Kawasaki, A. Ohtomo, T. Arakene, K. Takahashi, M. Yoshimoto, and H. Koinuma, Appl. Surf. Sci. **107**, 102 (1996).
[15] G. Koster, B. L. Kropman, G. J. H. M. Rijnders, D. H. A. Blank, and H. Rogalla, Appl. Phys. Lett. **73**, 2920 (1998).
[16] Y. Mukunoki, N. Nakagawa, T. Susaki, and H. Y. Hwang, Appl. Phys. Lett. **86**, 171908 (2005).
[17] T. Tomio, H. Miki, H. Tabata, T. Kawai, and S. Kawai, J. Appl. Phys. **76**, 5886 (1994).
[18] W. Ramadan, S. B. Ogale, S. Dhar, S. X. Zhang, D. C. Kundaliya, I. Satoh, and T. Venkatesen, Appl. Phys. Lett. **88**, 142903 (2006).
[19] A. Gupta and J. Z. Sun, J. Magn. Magn. Mater. **200**, 24 (1999).
[20] M. Bowen, A. Barthelemy, M. Bibes, E. Jacquet, J.-P. Contour, A. Fert, F. Ciccacci, L. Duo, and R. Bertacco, Phys. Rev. Lett. **95**, 137203 (2005).
[21] M. Bowen, M. Bibes, A. Barthelemy, J. P. Contour, A. Anane, Y. Lemaitre, and A. Fert, Appl. Phys. Lett. **82**, 233 (2003).
[22] C. H. Ahn, J.-M. Triscone, and J. Mannhart, Nature (London) **424**, 1015 (2003).
[23] C. H. Ahn, A. Bhattacharya, M. Di Ventra, J. N. Eckstein, C. D. Frisbie, M. E. Gershenson, A. M. Goldman, I. H. Inoue, J. Mannhart, A. J. Millis, A. F. Morpurgo, D. Natelson, and J.-M. Triscone, Rev. Mod. Phys. **78**, 1185 (2006).
[24] A. Bhattacharya, M. Eblen-Zayas, N. E. Staley, W. H. Huber, and A. M. Goldman, Appl. Phys. Lett. **85**, 997 (2004).
[25] M. Eblen-Zayas, A. Bhattacharya, N. E. Staley, A. L. Kobrinskii, and A. M. Goldman, Phys. Rev. Lett. **94**, 037204 (2005).
[26] X. X. Xi, J. Supercond. **7**, 137 (1994).
[27] A. Ohtomo and H. Y. Hwang, Nature (London) **427**, 423 (2004).
[28] W. Siemons, G. Koster, H. Yamamoto, W. A. Harrison, G. Lucovsky, T. H. Geballe, D. H. A. Blank, and M. R. Beasley, Phys. Rev. Lett. **98**, 196802 (2007).
[29] G. Herranz, M. Basletic, M. Bibes, C. Carretero, E. Tafra, E. Jacquet, K. Bouzehouane, C. Deranlot, A. Hamzic, J. M. Broto, A. Barthelemy, and A. Fert, Phys. Rev. Lett. **98**, 216803 (2007).
[30] M. Basletic, J.-L. Maurice, C. Carretero, G. Herranz, O. Copie, M. Bibes, E. Jacquet, K. Bouzehouane, S. Fusil, and A. Barthelemy, Nature Mater. **7**, 621 (2008).
[31] J. H. Haeni, P. Irvin, W. Chang, R. Uecker, P. Reiche, Y. L. Li, S. Choudhury, W. Tian, M. E. Hawley, B. Craigo, A. K. Tagantsev, X. Q. Pan, S. K. Streiffer, L. Q. Chen, S. W. Kirchoefer, J. Levy, and D. G. Schlom, Nature (London) **430**, 758 (2004).
[32] C. Lee, J. Destry, and J. L. Brebner, Phys. Rev. B **11**, 2299 (1975).
[33] S. Ohta, T. Nomura, H. Ohta, and K. Koumoto, J. Appl. Phys. **97**, 034106 (2005).
[34] C. Q. Tang, Z. Xia, S. Yao, and S. Chen, Cryst. Res. Technol. **31**, 821 (1996).
[35] O. N. Tufte and P. W. Chapman, Phys. Rev. **155**, 796 (1967).
[36] O. N. Tufte and E. L. Stelzer, Phys. Rev. **173**, 775 (1968).
[37] B. Gregory, J. Arthur, and G. Seidel, Phys. Rev. B **19**, 1039 (1979).
[38] H. P. R. Frederikse, W. R. Thurber, and W. R. Hosler, Phys. Rev. **134**, A442 (1964).
[39] S. Shapiro, Phys. Rev. **140**, A169 (1965).
[40] J. E. Carnes and A. M. Goodman, J. Appl. Phys. **38**, 3091 (1967).
[41] D. Parker and J. Yahia, Phys. Rev. **169**, 605 (1968).
[42] C. Lee, J. Yahia, and J. L. Brebner, Phys. Rev. B **3**, 2525 (1971).
[43] D. D. Sarma, S. R. Barman, H. Kajueter, and G. Kotliar, Europhys. Lett. **36**, 307 (1996).
[44] D. A. Crandles, B. Nicholas, C. Dreher, C. C. Homes, A. W. McConnell, B. P. Clayman, W. H. Gong, and J. E. Greedan, Phys. Rev. B **59**, 12842 (1999).
[45] T. Fix, R. Bali, N. Stelmashenko, and M. Blamire, Solid State Commun. **146**, 428 (2008).
[46] S. Dai, H. Lu, F. Chen, Z. Chen, Z. Ren, and D. Ng, Appl. Phys. Lett. **80**, 3545 (2002).
[47] Q. Zhou, K. Jin, H. Lu, P. Han, Z. Chen, K. Zhao, Y. Zhou, and G. Yang, Europhys. Lett. **71**, 283 (2005).
[48] G. Z. Yang, H. B. Lu, F. Chen, T. Zhao, and Z. H. Chen, J. Cryst. Growth **227-228**, 929 (2001).

[49] D. Fagg, V. Kharton, A. Kovalevsky, A. Viskup, E. Naumovich, and J. Frade, J. Eur. Ceram. Soc. **21**, 1831 (2001).
[50] A. Ferreira, J. Abrantes, J. Jurado, and J. Frade, Solid State Ionics **135**, 761 (2000).
[51] C. Shin, H. Yoo, and C. Lee, Solid State Ionics **178**, 1081 (2007).
[52] E. M. Conwell and V. F. Weisskopf, Phys. Rev. **77**, 388 (1950).
[53] H. Brooks, in *Advances in Electronics and Electron Physics*, edited by L. Marton (Academic Press, New York, 1955), Vol. 7, pp. 85-182.; C. Herring (unpublished).
[54] See the following paper which employed the results of an earlier theoretical treatment (Ref. 55) of the problem: A. L. Kholkin, E. V. Kuchis, and V. Trepakov, Ferroelectrics **83**, 135 (1988).
[55] Yu. N. Epifanov, A. P. Levanyuk, and G. M. Levanyuk, Ferroelectrics **35**, 199 (1981); **43**, 191 (1982).
[56] Yu. N. Epifanov and A. P. Levanyuk, Sov. Phys. Solid State **21**, 516 (1979).
[57] J. F. Schooley, W. R. Hosler, and M. Cohen, Phys. Rev. Lett. **12**, 474 (1964).
[58] C. S. Koonce, M. L. Cohen, J. F. Schooley, W. R. Hosler, and E. R. Pfeiffer, Phys. Rev. **163**, 380 (1967).
[59] P. Calvani, M. Capizzi, F. Donato, S. Lupi, P. Maselli, and D. Peschiaroli, Phys. Rev. B **47**, 8917 (1993).
[60] A. Ohtomo and H. Y. Hwang, J. Appl. Phys. **102**, 083704 (2007).
[61] K. Ueno, S. Nakamura, H. Shimotani, A. Ohtomo, N. Kimura, T. Nojima, H. Aoki, Y. Iwasa, and M. Kawasaki, Nature Mater. **7**, 855 (2008).
[62] Y. Kozuka, M. Kim, C. Bell, B. G. Kim, Y. Hikita, and H. Y. Hwang, Nature (London) **462**, 487 (2009).
[63] Y. Kozuka, T. Susaki, and H. Y. Hwang, Phys. Rev. Lett. **101**, 096601 (2008).
[64] Y. Kozuka, Y. Hikita, T. Susaki, and H. Y. Hwang, Phys. Rev. B **76**, 085129 (2007).
[65] Crystal GmbH, Berlin, Germany.
[66] MTI Corporation, Richmond, California, USA.
[67] N.-H. Chan, R. K. Sharma, and D. M. Smyth, J. Electrochem. Soc. **128**, 1762 (1981).
[68] X. D. Zhu, Y. Y. Fei, H. B. Lu, and G. Z. Yang, Appl. Phys. Lett. **87**, 051903 (2005).
[69] H. Yamada and G. R. Miller, J. Solid State Chem. **6**, 169 (1973).
[70] W. Gong, H. Yun, Y. B. Ning, J. E. Greedan, W. R. Datars, and C. V. Stager, J. Solid State Chem. **90**, 320 (1991).
[71] K. Szot, W. Speier, R. Carius, U. Zastrow, and W. Beyer, Phys. Rev. Lett. **88**, 075508 (2002).
[72] K. Szot, W. Speier, G. Bihlmayer, and R. Waser, Nature Mater. **5**, 312 (2006).
[73] K. Szot and W. Speier, Phys. Rev. B **60**, 5909 (1999).
[74] G. A. Thomas, A. Kawabata, Y. Ootuka, S. Katsumoto, S. Kobayashi, and W. Sasaki, Phys. Rev. B **26**, 2113 (1982).
[75] Y. Ootuka, H. Matsuoka, and S. Kobayashi, in *Anderson Localization*, edited by T. Ando and H. Fukuyama (Springer-Verlag, New York, 1987).
[76] P. Dai, Y. Zhang, and M. P. Sarachik, Phys. Rev. B **45**, 3984 (1992).
[77] P. A. Lee and T. V. Ramakrishnan, Rev. Mod. Phys. **57**, 287 (1985).
[78] B. L. Altshuler and A. G. Aranov, in *Electron-Electron Interactions in Disordered Systems*, edited by A. L. Efros and M. Pollak (Elsevier, Amsterdam, 1985), p. 1.
[79] H. Fukuyama, in *Electron-Electron Interactions in Disordered Systems* (Ref. 78), p. 155.
[80] B. I. Shklovskii and A. L. Efros, *Electronic Properties of Doped Semiconductors* (Springer-Verlag, New York, 1984).
[81] G. Bergmann, Phys. Rep. **107**, 1 (1984).
[82] These are approximate values. Exact values depend on the specific dopant (Ref. 83).
[83] N. F. Mott, *Metal-Insulator Transitions*, 2nd ed. (Taylor & Francis, London, 1990).
[84] M. Schultz and L. Lein, Appl. Phys. Lett. **91**, 151104 (2007).
[85] H. Nakamura, H. Takagi, I. H. Inoue, Y. Takahashi, T. Hasegawa, and Y. Tokura, Appl. Phys. Lett. **89**, 133504 (2006).
[86] J. G. Bednorz and K. A. Muller, Phys. Rev. Lett. **52**, 2289 (1984).
[87] I. Burn and S. Neirman, J. Mater. Sci. **17**, 3510 (1982).
[88] W.-D. Yang, K.-M. Hung, and C.-F. Kao, Ceram. Int. **26**, 475 (2000).
[89] A. E. Paladino, L. G. Rubin, and J. S. Waugh, J. Phys. Chem. Solids **26**, 391 (1965).
[90] W. H. Rhodes and W. D. Kingery, J. Am. Ceram. Soc. **49**, 521 (1966).
[91] D. L. Dexter and F. Seitz, Phys. Rev. **86**, 964 (1952).
[92] W. T. Read, Philos. Mag. **45**, 775 (1954); **45**, 1119 (1954); **46**, 111 (1955).
[93] J. B. Choi, S. Liu, and H. D. Drew, Phys. Rev. B **43**, 4046 (1991).
[94] J. J. Harris, T. Zhang, W. R. Branford, S. K. Clowes, M. Debnath, A. Bennett, C. Roberts, and L. F. Cohen, Semicond. Sci. Technol. **19**, 1406 (2004).
[95] L. Solymar and D. Walsh, *Electrical Properties of Materials*, 7th ed. (Oxford University Press, Oxford, 2004).
[96] N. F. Mott and E. A. Davis, *Electronic Processes in Non-Crystalline Solids* (Oxford University Press, Oxford, 1979).
[97] D. Romero, M.-W. Lee, H. D. Drew, M. Shayegan, and B. S. Elman, in *Anderson Localization*, edited by T. Ando and H. Fukuyama (Springer-Verlag, New York, 1987).
[98] C. J. Yeager and S. S. Courts, IEEE Sens. J. **1**, 352 (2001).
[99] L. G. Rubin, Cryogenics **37**, 341 (1997).
[100] Lake Shore Cryotronics Inc., Westerville, Ohio, USA.
[101] D. W. Denlinger, E. N. Abarra, K. Allen, P. W. Rooney, M. T. Messer, S. K. Watson, and F. Hellman, Rev. Sci. Instrum. **65**, 946 (1994).
[102] S. L. Lai, G. Ramanath, L. H. Allen, P. Infante, and Z. Ma, Appl. Phys. Lett. **67**, 1229 (1995); S. L. Lai, G. Ramanath, L. H. Allen, and P. Infante, *ibid.* **70**, 43 (1997).
[103] B. L. Zink, E. Janod, K. Allen, and F. Hellman, Phys. Rev. Lett. **83**, 2266 (1999).
[104] B. Revaz, M.-C. Cyrille, B. L. Zink, I. K. Schuller, and F. Hellman, Phys. Rev. B **65**, 094417 (2002).
[105] B. L. Zink, R. Pietri, and F. Hellman, Phys. Rev. Lett. **96**, 055902 (2006).
[106] D. Querlioz, E. Helgren, D. R. Queen, F. Hellman, R. Islam, and D. J. Smith, Appl. Phys. Lett. **87**, 221901 (2005).
[107] D. R. Queen and F. Hellman, Rev. Sci. Instrum. **80**, 063901 (2009).
[108] E. Ramsden, *Hall Effect Sensors: Theory and Application* (Elsevier, New York, 2006).